analytical chemistry

pubs.acs.org/ac

Article

Profiling Glucose-Stimulated and M3 Receptor-Activated Insulin Secretion Dynamics from Islets of Langerhans Using an Extended-Lifetime Fluorescence Dye

Joel E. Adablah, Yao Wang, Matthew Donohue, and Michael G. Roper*

Cite This: *Anal. Chem.* 2020, 92, 8464−8471

Read Online

ACCESS | Metrics & More | Article Recommendations | Supporting Information

ABSTRACT: Pulsatile insulin from pancreatic islets is crucial for glucose homeostasis, but the mechanism behind coordinated pulsatility is still under investigation. One hypothesis suggests that cholinergic stimulation of islets by pancreatic ganglia resets these endocrine units, producing synchronization. Previously, it was shown that intracellular Ca^{2+} oscillations within islets can be entrained by pulses of a cholinergic agonist, carbachol (CCh). Although these proxy measurements of Ca^{2+} provided insight into the synchronization mechanism, measurement of insulin output would be more direct evidence. To this end, a fluorescence anisotropy competitive immunoassay for online insulin detection from single and grouped islets in a microfluidic system was developed using a piezoelectric pressure-driven fluid delivery system and a squaraine rotaxane fluorophore, SeTau-647, as the fluorescent label for insulin. Due to SeTau-647 having a longer lifetime and higher brightness compared to the previously used Cy5 fluorophore, a 45% increase in the anisotropy range was observed with enhanced signal-to-noise ratio (S/N) of the measurements. This new system was tested by measuring glucose-stimulated insulin secretion from single and groups of murine and human islets. Distinct islet entrainment of groups of murine islets by pulses of CCh was also observed, providing further evidence for the hypothesis that pulsatile output from the ganglia can synchronize islet behavior. We expect that this relatively straightforward, homogeneous assay can be widely used for examining not only insulin secretion but other secreted factors from different tissues.

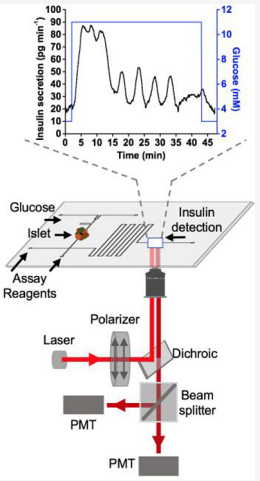

Recent years have brought new insights on the microstructure and innervation of the pancreas and its endocrine fraction, the islets of Langerhans.[1−3] Insulin release from single islets is pulsatile with a period of 3−7 min,[4−6] and similar periods have been reported in vivo when insulin levels are measured in the portal vein.[7,8] For an oscillatory insulin profile to be observed in vivo, the release of insulin from a large majority of islets within the pancreas must be synchronized, yet how this synchronization occurs is still unclear. It is clear, however, that these in vivo oscillations are important, as disordered oscillations are observed in individuals prior to, and during, Type 2 diabetes,[9] and these dynamic insulin profiles act more efficiently than static levels on regulating glucose.[10,11]

One potential mechanism of how islets may be synchronized is by continuous resetting of islet oscillations due to repeated pulses of acetylcholine (ACh) from parasympathetic ganglia, clusters of autonomic nerve cell bodies that innervate the pancreas. ACh potentiates glucose-stimulated insulin secretion (GSIS) by activating M_3-muscarinic receptors (M3R) in islets. This activation leads to mobilization of Ca^{2+} from inositol-1,4,5-trisphosphate (IP_3)-sensitive Ca^{2+} stores in the endoplasmic reticulum and the acceleration of protein kinase C-mediated insulin exocytosis.[12,13]

This hypothesis to explain islet synchronicity has been supported by the observation of spontaneous bursts of electrical activity in ganglia of a feline pancreas every 6−8 min,[14] correlating with the insulin oscillation periods found in plasma. In addition, insulin oscillations at a similar period have been observed during ex vivo perfusion of the pancreas,[7,15−17] implying the synchronizing agent must be local to the pancreas. In vitro studies have also shown that a single pulse of ACh or the M3R agonist carbachol (CCh) can promote transient synchronization in groups of murine islets in a glucose-rich environment.[18,19] Building on these findings, we found that groups of murine islets exposed to periodic or aperiodic pulses of CCh can be synchronized.[20] However, the only evidence reported has been the synchronization of intracellular Ca^{2+} oscillations as a marker of insulin release with no report demonstrating synchronized, oscillatory hormone release.

To shed light on how M3R activation may synchronize insulin secretion, the development and use of high-sensitivity and high temporal resolution analytical methods are essential. The most established methods for insulin measurement are heterogeneous

Received: March 20, 2020
Accepted: May 20, 2020
Published: May 20, 2020

antibody-based assays, chief among which are enzyme-linked immunosorbent assays (ELISAs). These heterogeneous assays have high sensitivity, yet typically require multiple wash steps, forcing the assays to be offline due to their long processing times. Other types of immunoassays have been developed to limit these drawbacks, for example, by incorporating electrophoretic immunoassays into microfluidic systems.[5,6,21−23] While this type of analysis has many advantages over ELISA, including the ability to perform online measurements, there are several drawbacks to the method that limit its incorporation into other laboratories. Perhaps the biggest obstacle is working with shallow microfluidic channels with depths less than 10 μm. These small channel dimensions are required to reduce the electric current and subsequent Joule heating to acceptable levels, but also lead to more arduous channel fabrication processes and higher risks of clogging.

In contrast, homogeneous immunoassays do not require a wash or separation step, easing the requirements for the channel dimensions. Several homogeneous-based approaches have been described,[24−31] with only a few being utilized for online measurement of insulin release in microfluidic systems.[28−30] Fluorescence anisotropy (or fluorescence polarization) immunoassays have been used for detection of antibodies or antigens in biological samples for decades.[32−34] Fluorescence anisotropy is a measure of the depolarization of fluorescence emission that occurs after a fluorophore has been excited by linearly polarized light.[34] Immunoassays using this detection system are typically competitive, whereby the target and a tagged analogue of the target compete for binding sites to a limited amount of antibody. In the case of insulin measurements, insulin (Ins) released from islets competes with fluorescently tagged insulin (Ins*) for a limiting amount of anti-insulin antibody (Ab_{Ins}). Quantification necessitates measuring the amount of antibody-bound (B) and free (F) tagged species (Ins*), with the B/F ratio inversely related to the concentration of target (Ins) in the mixture. This ratio is determined using fluorescence anisotropy because each of these species has a unique anisotropy as seen by the Perrin equation:

$$r = \frac{r_0}{1 + \tau/\theta} \tag{1}$$

where r_0 is the fundamental anisotropy of the fluorophore, τ is its fluorescence lifetime, and θ is its rotational correlation time, defined as

$$\theta = \frac{\eta \overline{V}}{RT} \tag{2}$$

where η is viscosity, $\overline{V}$ is the molar volume, R is the universal gas constant, and T is temperature. In the case of the competitive insulin immunoassay, the increased $\overline{V}$ of the bound Ins*−Ab_{Ins} complex compared to free Ins* leads to a higher anisotropy for the bound species (r_B) than for the free Ins* (r_F). The immunoassay can be performed homogeneously because the total anisotropy ($\langle r \rangle$) of the mixture is a sum of r_B and r_F weighted by their fractional amounts:

$$\langle r \rangle = f_B r_B + f_F r_F \tag{3}$$

where f_B and f_F are the fractional amount of B and F Ins*, respectively. Every insulin concentration results in a unique combination of f_B and f_F, and therefore, a distinct $\langle r \rangle$. The competitive assay is ideal for this measurement technique due to the large differences in $\overline{V}$ between the B and F Ins*. The $\langle r \rangle$ is determined experimentally by exciting the solution with linearly polarized light and measuring the degree of depolarization in the emission normalized to the total fluorescence emission:

$$\langle r \rangle = \frac{I_{\parallel} - I_{\perp}}{I_{\parallel} + 2I_{\perp}} \tag{4}$$

with $I_{\parallel}$ and $I_{\perp}$ representing the fluorescence emission intensities parallel and perpendicular, respectively, to the polarization of the excitation light. Equation 4 assumes equal detection sensitivity for the two polarization states.

We have recently applied this methodology to monitor GSIS from single and multiple islets of Langerhans using Cy5-labeled insulin as Ins*.[28,29,35] In this report, we describe the improvement of this previous assay using a brighter fluorophore with a longer lifetime than Cy5. To demonstrate this new system, similar GSIS dynamics were observed from murine and human islets to those found using other analytical techniques. We then used the method to provide the first reported evidence of coordinated insulin pulses from batches of islets in response to periodic stimulation by CCh. These applications not only show the benefit of this microfluidic-based approach for measuring insulin release from either single or groups of islets but also provide further evidence that cholinergic release from parasympathetic nerves may help to coordinate islet behavior resulting in periodic pulses of insulin.

EXPERIMENTAL SECTION

Chemicals and Reagents. All reagents for microfluidic assays and isolation and culture of islets were obtained from Sigma-Aldrich (St. Louis, MO, U.S.A.) unless otherwise stated. NaOH, KCl, Tween-20, KCl, and HF were from EMD Chemicals (San Diego, CA, U.S.A.). Glucose (dextrose), RPMI 1640, and gentamicin sulfate were from Thermo Fisher Scientific (Waltham, MA, U.S.A.). Collagenase P (from *Clostrdium histolyticum*) was acquired from Roche Diagnostics (Indianapolis, IN, U.S.A.). Cosmic Calf Serum was acquired from GE Healthcare Bio-Sciences (Pittsburgh, PA, U.S.A.). Monoclonal Ab_{Ins} was purchased from Meridian Life Science, Inc. (Saco, ME, U.S.A.). All solutions were made with Milli-Q (Millipore, Bedford, MA, U.S.A.) 18 MΩ·cm ultrapure water and filtered using 0.2 μm nylon syringe filters (Pall Corporation, Port Washington, NY, U.S.A.). Immunoassay reagents (Ins* and Ab_{Ins}) were prepared in TEAT-40 composed of 25 mM Tricine, 40 mM NaCl, 1 mM EDTA at pH 7.4 with an additional 0.1% Tween-20 (w/v) and 1 mg mL^{-1} BSA. A balanced salt solution (BSS) made to pH 7.4 was used for preparing Ins standards and for islet perfusion. BSS was composed of 125 mM NaCl, 2.4 mM $CaCl_2$, 1.2 mM $MgCl_2$, 5.9 mM KCl, 25 mM HEPES, 1 mg mL^{-1} BSA, and 3, 11, or 12 mM glucose. Reagents for isolation and culture of murine islets were prepared as previously described.[36]

Insulin Labeling and Purification of SeTau-647-Labeled Insulin. Labeling Ins with SeTau-647-NHS (SETA BioMedicals, Urbana, IL, U.S.A.) and purifying Ins* involved chromatographic purification followed by confirmation of antibody binding by capillary electrophoresis (CE), adapted from what has been described previously for Cy5-labeled Ins.[37] Briefly, 1 mg of bovine insulin in 0.1 M $NaHCO_3$ (pH 9.3) was added to a vial containing 1 mg of SeTau-647. The mixture was incubated in the dark at room temperature for 30 min with gentle stirring every 5 min. The mixture was then separated using a PD-10 desalting column (GE Healthcare Bio-Sciences). The first visibly eluting band was collected and purified.

https://dx.doi.org/10.1021/acs.analchem.0c01226
Anal. Chem. 2020, 92, 8464−8471

Further purification of this band was performed by liquid chromatography (LC) using a Beckman 127S solvent module pump and a Beckman 166 UV detector (Beckman Coulter, Brea, CA, U.S.A.). The column was a 25 cm × 4.6 mm i.d. Symmetry300 C4 (Waters Corp., Milford, MA, U.S.A.) with a particle diameter of 5 μm. Separation was performed using 70% water containing 0.1% trifluoracetic acid (TFA)/30% acetonitrile with 0.1% TFA with UV−vis detection at 280 nm. Injections of 200 μL were made onto the column, and all detected peaks were collected.

The same peaks from multiple LC runs were pooled and concentrated to dryness (Savant Speedvac, Thermo Fisher Scientific). Each pooled fraction was checked for binding to Ab_{Ins} by adding enough Ab_{Ins} in TEAT-40 to produce a 24 nM final concentration. The resulting mixture was separated by CE (Beckman Coulter) with a 25 μm i.d. × 60 cm fused-silica capillary (Polymicro Technologies, Phoenix, AZ, U.S.A.) using a 20 kV separation potential. Detection was accomplished using laser-induced fluorescence with a 635 nm laser (AixiZ, Houston, TX, U.S.A.) and a 663 nm long-pass filter. Separation buffer contained 150 mM Tricine and 20 mM NaCl made to pH 7.4. After determining which fraction bound to Ab, the Ins* was quantified by UV−vis spectroscopy using the molar extinction coefficient of SeTau-647 (ϵ = 200 000 M^{-1} cm^{-1} at 649 nm). Labeled insulin was aliquoted and stored in the dark at −80 °C. Each aliquot contained 2.5 μL of 20 μM Ins* which was then diluted to 45 nM in TEAT-40 for microfluidic experiments.

Microfluidic Device and System. The microfluidic device was fabricated in borosilicate glass using photolithography and wet etching techniques as previously detailed.[37,38] Microfluidic channels were 90 μm × 195 μm (depth × width at middle) as measured by an SJ-410 surface profiler (Mitutoyo Corp., Aurora, IL, U.S.A.). Fluidic inputs and the 120 nL islet chamber were drilled using 0.02 in. and 0.012 in. diamond-tipped drill bits, respectively (Wolfco Inc., Bozrah, CT, U.S.A.). The device had four fluidic inlets: the two upstream of the islet chamber delivered BSS with different concentrations of secretagogues, while the two inlets downstream of the islet chamber delivered 45 nM Ins* and 90 nM Ab_{Ins}, both in TEAT-40. Each inlet was connected to a fluid reservoir pressurized by a piezoelectric flow controller (Elvesys, Paris, France) with their flow rates regulated by in-line flow sensors (Elvesys). The error associated with these sensors was specified at 2% RSD by the manufacturer and was periodically verified. The final Ins* and Ab_{Ins} concentrations were determined by the ratio of flow rates from each of these inlets to the total flow rate. Throughout the remainder of the text, the concentrations of the immunoassay reagent are given which correspond to the fully mixed species.

Temperature Control. To ensure physiological temperature within the islet chamber, the entire microfluidic device was secured in the center of a custom-built copper plate with 2 mm wide slits cut in the shape of the channels to allow for optical detection within the device.[28] On each corner of the plate, a thermoelectric (Peltier) heater (TEC1-12706, Hebeit I.T., Shanghai, China) was attached using a thermal adhesive paste (Arctic Silver Inc., Visalia, CA, U.S.A.). On the opposite side of each Peltier was attached a 40 mm × 40 mm × 10 mm (L × W × D) aluminum heat sink. Each Peltier was powered by an 18 V, 3 A power supply (Extech Instruments, Nashua, NY, U.S.A.). For temperature measurement, a calibrated T-240C microthermocouple (Physitemp Instrument, Inc. Clifton, NJ, U.S.A.) connected to a TAC80B-T thermocouple-to-analog converter (Omega Engineering, Inc., Stamford, CT, U.S.A.) was sandwiched between the copper plate and microfluidic device. The temperature was input into a LabView program (National Instruments, Austin, TX, U.S.A.) written in house via an NI-PCIe 6321 data acquisition (DAQ) card (National Instruments). The program, through the DAQ card and a Crydom CMX60D10 relay, interrupted the power supply to the Peltier circuit to maintain the desired temperature. Islet chamber temperature throughout a typical 60 min experiment was measured to be 37.0 ± 0.3 °C.

Optical Detection System for the Microfluidic Device. A 635 nm laser (Coherent Inc. Santa Clara, CA, U.S.A.) was used as the excitation source. The laser power was reduced from 25 to 7.8 mW with a neutral density filter (Thorlabs Inc., Newton, NJ, U.S.A.). An achromatic fiberport collimator (PAF2S-7A, Thorlabs) coupled the attenuated beam into a multimode fiber-optic bundle (Ceramoptec, Sunnyvale, CA, U.S.A.) which then fed into a telescoping lens tube (SM1NR1, Thorlabs). Contained in the lens tube was an achromatic doublet (AC254-080-A-ML, Thorlabs) to collimate the excitation beam followed by a quartz-wedge achromatic depolarizer (DPU-25-A, Thorlabs) to randomize the optical polarization of the beam. The beam entered the back of an Eclipse TS-100 microscope (Nikon Instruments Inc., Melville, NY, U.S.A.), was polarized in the desired orientation using a linear polarizer (WP25M-VIS, Thorlabs), and reflected by a dichroic mirror (XF2035, Omega Optical Inc., Brattleboro, VT, U.S.A.). The reflected light was focused by a 40×, 0.6 NA objective (Nikon) into the microfluidic channel at the detection point. Fluorescence emission was collected with the same objective, transmitted through the dichroic, and directed into a two-channel microscope photometer (Horiba Scientific, Piscataway, NJ, U.S.A.). Within the photometer, the light passed through a spatial filter, a 665 nm long-pass filter (HQ665LP, Chroma Technology Corp., Bellows Falls, VT, U.S.A.), and a 635 nm notch filter (ZET635NF, Chroma Technology Corp.). The emission beam was split by a polarizing beam splitter cube (PBS101, Thorlabs) into its parallel and perpendicular polarized components (with respect to the excitation polarization). Each polarized component passed through a complementary linear polarizer prior to impinging on separate photomultiplier tubes (PMTs) (R10699, Hamamatsu Photonics, Middlesex, NJ, U.S.A.). Because most of the fluorescence emission collected by the objective was parallel to the polarization axis of the excitation beam, the gain of the PMT for detection of the perpendicular component was set to 0.1 μA V^{-1}, whereas the gain for the PMT used for detection of the parallel component was 1.0 μA V^{-1}. Data from both PMTs were collected at 1000 Hz with a DAQ card (National Instruments, USB 6009) using a LabView program written in house.

Procurement and Culture of Islets. The islet isolation protocol was approved by the Florida State University Animal Care and Use Committee (Protocol 1813) in a similar manner as previously reported.[35−38] Islets from two mice were pooled and incubated in RPMI 1640 containing 11 mM glucose, L-glutamine, 10% Cosmic Calf serum, 100 U mL^{-1} penicillin, 100 μg mL^{-1} streptomycin, and 10 μg mL^{-1} gentamycin at 37 °C and 5% CO_2. Islets were used no more than 4 days after isolation. Prior to each experiment, islets were rinsed in BSS containing 3 mM glucose for at least 5 min before loading into the islet chamber by sedimentation with a pipette. After loading, the islet chamber was sealed with a piece of adhesive PCR film.

Human islets, procured from Prodo Laboratories (Aliso Viejo, CA, U.S.A.), were obtained from a deidentified cadaveric organ

https://dx.doi.org/10.1021/acs.analchem.0c01226
Anal. Chem. 2020, 92, 8464−8471

donor and, therefore, were exempt from Institutional Review Board approval. The donor was a 40 year old Hispanic female, 67 in., 203 lbs., 31.8 BMI, 4.8% HbA1c, and without a history of diabetes. Culture of human islets was performed at 37 °C and 5% CO_2 in PIM(S) islet-specific media (Prodo Laboratories).

Data Analysis. Data collected from both PMTs during experiments were converted to anisotropy using eq 4. Anisotropy traces were smoothed by a 1000-point moving boxcar average. To quantify insulin, online calibration curves were performed using 24 nM Ins* and Ab_{Ins} and 0−400 nM insulin for experiments with multiple islets. For single-islet experiments, the insulin concentrations were halved and immunoassay reagent concentrations were reduced to 18 nM. Calibration curves were generated after islet experiments and were performed at 37 °C. Each point on a curve was the average anisotropy after a 1 min collection with error bars representing ±1 standard deviation (SD). Calibration points were fitted to a four-parameter logistic curve. The equation from the curve was used to convert anisotropy to an insulin concentration that was subsequently normalized by the flow rate through the islet chamber. Limit of detection (LOD) was taken as the concentration of insulin required to decrease anisotropy to a value lower than 3 times the SD of the blank. For single and grouped islet experiments, LOD was 10 and 20 nM, respectively, due to the different immunoassay reagent concentrations used for the experiments. All error bars are ±1 SD unless indicated otherwise. The amount of insulin released from islets was quantified by measuring the area under the curve for specified durations using Origin 9.0 (OriginLab, Northampton, MA, U.S.A.).

RESULTS AND DISCUSSION

Fluorescence anisotropy is an all-optical, quantitative method for analysis of the degree of rotational depolarization of a fluorophore. For decades, this technique (or a similar technique, fluorescence polarization) has been used for quantitative measurements of homogeneous immunoassays, typically in plate reader-based systems.[32−34] Using this method in a flow-based system allows dynamic concentration changes to be identified without the need for separation of the B and F Ins*. We have previously developed a fluorescence anisotropy immunoassay for quantification of insulin release from islets using Cy5−insulin as the labeled Ins* and gravity as the means to drive fluid flow in the device.[28,39] In this report, we describe the use of SeTau-647 as the fluorescent label for Ins*, which provided a larger dynamic range to the insulin assay compared to Cy5, and an actively controlled perfusion system that improved the robustness of the device and resulted in an increased temporal resolution of the assay.

Microfluidic Device and Perfusion System Characterization. In the previous iteration of the system,[28] gravity-driven flow was used to deliver reagents to the microfluidic chip. Although there are several advantages to this passive pressure-driven mechanism of fluid delivery, one major drawback is its inability to automatically correct flow rate fluctuations when bubbles or clogs develop in the fluidic lines or microfluidic device. To improve the robustness of flow, a variable-pressure system was implemented. Presented in Figure S1 is a schematic of the fluidic control system. Fluid reservoirs containing assay reagents were pressurized with filtered air by a piezoelectric pressure regulator. As liquid flowed from the reservoirs into the microfluidic device, flow rates were continuously monitored by an in-line flow sensor connected in a feedback loop to the piezoelectric regulator which adjusted the pressure output to maintain flow stability. In Figure 1A, the positions of fluidic

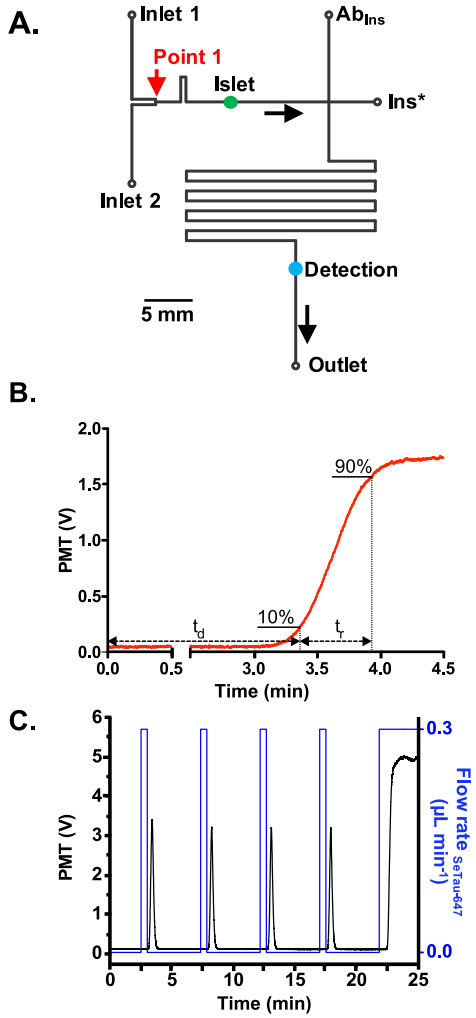

Figure 1. Microfluidic chip, flow profile, and pulse train characterization. (A) Perfusion solutions or insulin standards were delivered to inlets 1 and 2 for islet experiments or calibrations, respectively, and passed through the closed islet chamber (green dot). The two remaining inlets were used to deliver Ab_{Ins} and Ins* as noted. The reagents mixed and equilibrated in the 160 mm long mixing channel before fluorescence measurement at the detection point (blue dot). Black arrows indicate the direction of flow. (B) Flow of SeTau-647 was initiated from at 0 min, while signal was measured at the detection point. The *x*-axis break at 0.5 min is for ease in viewing. (C) The blue trace (right axis) shows the programmed flow rates of SeTau-647 delivered from inlet 2. The black trace (left axis) is the fluorescence signal at the islet chamber during a pulsing experiment. A 53 ± 3% pulse attenuation was observed at the islet chamber.

ports, islet chamber (green dot), and detection point (blue dot) on the chip are annotated, together with the direction of flow. For all experiments, the perfusion flow rate through the islet chamber was maintained at 0.3 μL min^{-1}. The Ins* and Ab_{Ins} flow rates were set at 0.4 and 0.8 μL min^{-1}, respectively, for a total flow rate at the detection point of 1.5 μL min^{-1}.

The microfluidic system was held on the stage of a microscope, and the optical system (Figure S2) was used to evaluate the temporal resolution of the system. Reservoirs connected to inlets 1 and 2 contained BSS and 20 nM SeTau-647, respectively. BSS was delivered to the Ab_{Ins} and Ins* inlets

https://dx.doi.org/10.1021/acs.analchem.0c01226
Anal. Chem. 2020, 92, 8464−8471

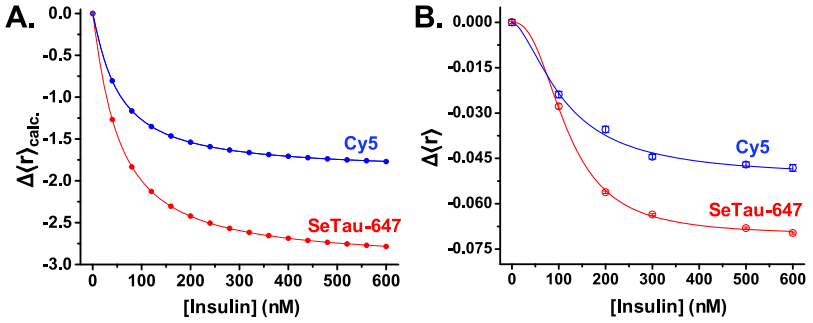

Figure 2. Competitive immunoassay improvement with squaraine rotaxane fluorophore. (A) Calculated calibration curves using Ins^*_{Cy5} and $Ins^*_{SeTau\text{-}647}$ were computed using their photophysical properties and mathematically calculated B/F ratios as explained in the text and Supporting Information. (B) Experimental calibration curves generated with 24 nM Ab_{Ins} and 24 nM of either Ins^*_{Cy5} or $Ins^*_{SeTau\text{-}647}$. $\Delta\langle r\rangle$ values in panels A and B are taken as relative to the anisotropy at 0 nM. SeTau-647 is shown to produce improved assay range from both calculated (panel A) and experimental (panel B) results.

(Figure 1A) at 0.4 and 0.8 μL min^{-1}, respectively, with the islet chamber sealed. Initially, BSS flowed into the device through inlet 1 at 0.3 μL min^{-1}, while the flow of SeTau-647 from inlet 2 was set to 0.0 μL min^{-1}. The flow rates from inlets 1 and 2 were then reversed so that SeTau-647 was delivered and fluorescence was measured at the detection point of the device. As shown in Figure 1B, after a delay time (t_d), the fluorescence increased until the signal plateaued. Because time 0 corresponded to the time at which SeTau-647 began to flow, t_d quantified the time for travel from point 1 in Figure 1A to the detection point. The t_d was determined as the intensity to reach 10% of the final signal at the detection point and was 3.2 ± 0.2 min (n = 4 trials). The response time (t_r) was the time required for the fluorescence signal to change from 10% to 90% of the final signal at the detection point. This value was 36 ± 1 s (n = 4), a 3-fold improvement on the previous gravity-driven perfusion system,[28] and was taken as the temporal resolution of the device. The values provided here are for trials within a single microfluidic device; the interdevice numbers varied slightly, but the intradevice variation was similar.

To evaluate how pulses of CCh would attenuate when delivered to the islet chamber, sequential pulses of SeTau-647 were produced and measured at the islet chamber. Initially, BSS was delivered through inlet 1 at 0.3 μL min^{-1}. The flow was then stopped, and SeTau-647 was delivered for 30 s through inlet 2. After the 30 s had elapsed, BSS was again delivered. This pattern was repeated every 4.5 min until four pulses of SeTau-647 were generated followed by a constant flow of SeTau-647. The PMT voltage (Figure 1C) showed the arrival of all four pulses as well as a plateau when constant dye was perfused. The delay time for travel between point 1 and the islet chamber was measured to be 0.71 ± 0.01 min (n = 4) using the pulse profile shown in Figure 1C. Due to travel through the channels during that time, a 53 ± 3% attenuation in signal was observed as measured by the height of the pulses as compared to the constant dye delivery.

Assay Improvement with Squaraine Rotaxane Fluorophore. Previously, Cy5 was used as the fluorescent label for Ins*.[28] Since fluorescence anisotropy is a spectroscopic measurement, the photophysical features of the fluorescent label play an important role in the assay. Therefore, we sought to replace Cy5 with a commercially available fluorescent label with superior optical properties. This new fluorophore, SeTau-647, is a squaraine rotaxane fluorescent probe which has similar excitation and emission maxima to Cy5 but a larger Stokes shift (46 nm), a larger molar extinction coefficient (200 000 M^{-1} cm^{-1}), a larger quantum yield (0.65), and a longer fluorescence lifetime (3.2 ns) in aqueous solutions.[40,41] Encapsulation of the squaraine chromophore by the rotaxane macrocycle provides protection of the dye, thereby increasing chemical stability and photobleaching resistance.[42]

To further justify switching the fluorophore, predicted immunoassay calibration curves were made by calculating the anisotropy ($\langle r\rangle_{calc}$) for Cy5-labeled Ins (Ins^*_{Cy5}) and SeTau-647-labeled Ins ($Ins^*_{SeTau\text{-}647}$) at different insulin concentrations. To perform these calculations, r_B and r_F for Ins^*_{Cy5} and $Ins^*_{SeTau\text{-}647}$ were calculated using eqs 1 and 2 with θ values for each species assuming 0 degrees of hydration and at 37 °C. Values for τ and r_0 were obtained from the literature.[43−46] Table S1 summarizes the properties of the B and F species for both labels used to calculate r_B and r_F. Once these two anisotropies were calculated, f_B and f_F at different unlabeled insulin concentrations were calculated using mass action and equilibrium equations (see the Supporting Information for details). These values were then used to determine $\langle r\rangle_{calc}$ using eq 3.

Figure 2A shows the calculated immunoassay calibration curves for both fluorophores. All data points were plotted relative to the anisotropy at 0 nM insulin, and both curves show the sigmoidal decrease in anisotropy as a function of insulin as expected for a competitive assay. To quantify assay improvement, the changes in anisotropies ($\Delta\langle r\rangle_{calc}$) for both curves from 0 to 600 nM insulin were compared. A 57% larger change was found with SeTau-647 compared to Cy5 due to the larger τ of the former. Conceptually, the larger value permits a higher degree of depolarization resulting in a greater change in anisotropy between r_B and r_F in eq 3.

Following these calculations, a comparison of experimentally obtained calibration curves using $Ins^*_{Cy\text{-}5}$ and $Ins^*_{SeTau\text{-}647}$ was made (Figure 2B). Measurements were relative to the mean anisotropy at 0 nM insulin. A 45% increase in the range of anisotropy values was observed with $Ins^*_{SeTau\text{-}647}$, similar to the calculated increase in anisotropy values. Additionally, due to the superior quantum yield of the squaraine rotaxane compared to Cy5, the signal-to-noise ratios (S/N) of the measurements were enhanced, resulting in a 44% decrease in the average SD across the 6-point calibration curves. The LOD, limited in competitive assays by the equilibrium constant of the antibody−antigen reaction, was 20 nM for both curves since both used the same Ab_{Ins}.

https://dx.doi.org/10.1021/acs.analchem.0c01226
Anal. Chem. 2020, 92, 8464−8471

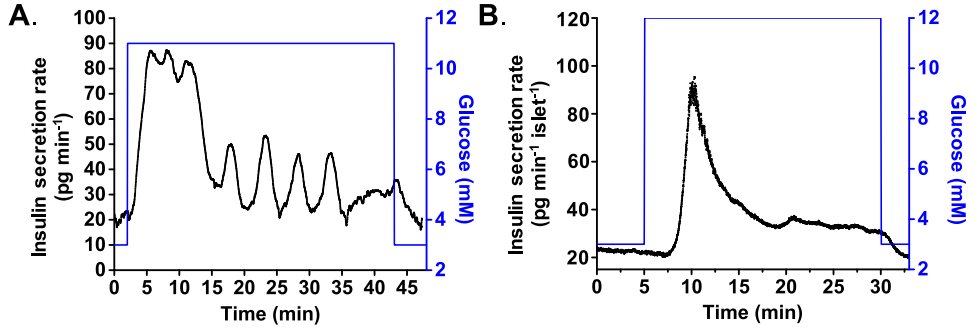

Figure 3. Online GSIS measurement from single and grouped murine islets. In both experiments, the black trace (left *y*-axis) is the insulin secretion rate per islet, whereas the blue profile (right axis) is the glucose stimulus. (A) A solution of 11 mM glucose was delivered for 40 min to a single murine islet during which biphasic, pulsatile insulin release was observed. (B) A group of five murine islets showed biphasic insulin secretion release during the 25 min exposure to 12 mM glucose.

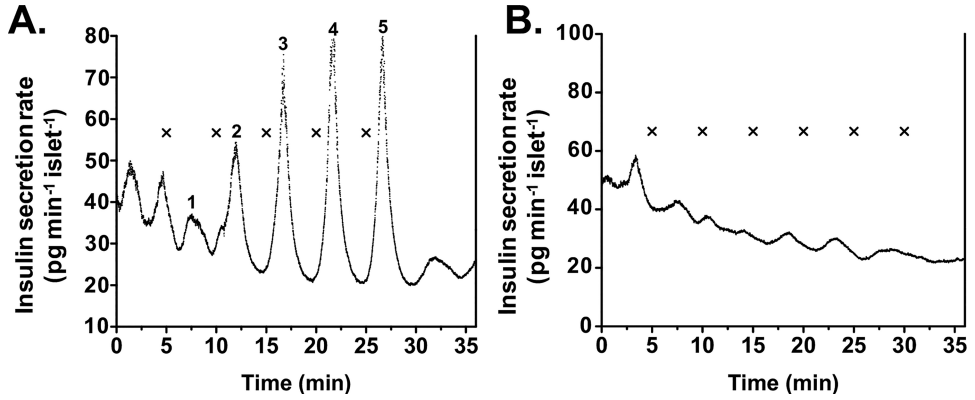

Figure 4. Entraining effect of periodic CCh pulses on GSIS in murine islets. In both panels, five murine islets were perfused with a constant 11 mM glucose concentration. (A) A train of five CCh pulses were delivered for 30 s each, every 5 min, as denoted by an "×". The numbered insulin peaks correlate to those mentioned in the text. (B) A representative control experiment is shown with flow switches denoted by "×". Because no CCh was present, no large pulses of insulin were observed.

Online Glucose Stimulated Insulin Secretion Measurements. Initial islet experiments were performed with murine islets to compare insulin secretion profiles using this new system to what has been reported previously.[5,6,22,23,37,38] For single-islet experiments, fluidic reservoirs leading to inlets 1 and 2 contained BSS with 3 and 11 mM glucose, respectively. After loading and sealing an islet in the microfluidic chamber, 3 mM glucose was applied for 5 min to condition the islet to flow. After this rinse, anisotropy measurements commenced with 3 mM glucose for 2 min, followed by 11 mM for 40 min, and then a return to 3 mM. Figure 3A shows a representative GSIS profile from a single murine islet. The black trace, corresponding to the left *y*-axis, represents the insulin profile; the blue trace, corresponding to the right *y*-axis, represents the glucose profile. During the initial 2 min perfusion with 3 mM glucose, 42 pg of insulin was released. Glucose was then increased to 11 mM, and a burst in insulin release followed. Over the initial 13 min of exposure to 11 mM glucose, 900 pg of insulin was released. After the initial burst, insulin was released in a pulsatile manner, consistent with other reports.[5,6,22,23,36] Over the next 28 min, 900 pg of insulin was secreted. The insulin release rate returned to basal levels when the glucose challenge was removed. Figure S3 shows the insulin secretion profiles of three additional murine islet GSIS experiments. Similar trends were observed with biphasic insulin release from each islet, although phase 2 oscillations were not as marked as that shown in Figure 3A.

A representative example of GSIS monitoring from a group of five murine islets in the microfluidic chamber is shown in Figure 3B. For this experiment, fluidic reservoirs connected to inlets 1 and 2 contained BSS with 3 and 12 mM glucose, respectively. The islets were rinsed with 3 mM glucose for 5 min resulting in 570 pg of insulin secreted. Glucose levels then rose to 12 mM for a total of 25 min. During the initial 13 min of high glucose exposure, 2900 pg of insulin was released followed by a more decreased output at 2000 pg for the remaining 12 min. Secretion rates returned to basal levels when glucose was lowered to 3 mM. Figure S4 shows three additional GSIS experiments. In each experiment, four islets were loaded into the chamber and exposed to 12 mM glucose. Biphasic insulin release was observed during the glucose challenges. For both single and multiple islet experiments, the insulin secretion rates per islet were comparable with previously reported values.[5,6,22,23,25,26,28,37,38]

Due to the increased significance in understanding the biology of human disease, we also tested the ability to measure GSIS from human islets using this system. As a representative case (Figure S5), three similarly sized (∼150 μm) islets from a healthy female donor were placed in the chamber and insulin secretion recorded for 2 min at 3 mM glucose. Insulin output was 100 pg during the low glucose rinse. GSIS was initiated by delivering 11 mM glucose for 15 min with a total of 1600 pg of insulin measured. Insulin secretion did not readily return to baseline levels with 3 mM glucose. This secretion profile for

https://dx.doi.org/10.1021/acs.analchem.0c01226
Anal. Chem. 2020, 92, 8464−8471

human islets is consistent with what has been observed previously.[29,47−50]

Thus far, we have shown the capabilities of the homogeneous, online fluorescence anisotropy competitive immunoassay to quantify biphasic GSIS dynamics from both single and grouped murine and human islets. The improved assay range and higher S/N offered by SeTau-647, as well as the subminute temporal resolution of this microfluidic system, allowed observations of insulin secretion dynamics that were previously unobservable in most homogeneous assays[24−29] except the most recently reported droplet-based molecular pincer assay.[30]

Repetitive Activation of M3 Receptors Synchronize Murine Islets. CCh, an M3R agonist, synchronizes glucose-induced islet activity as measured by synchronized oscillations of $[Ca^{2+}]_i$ levels.[18−20] Because no recording of insulin release has been reported after delivery of CCh pulses, synchronized hormone secretion is yet to be verified. Using the newly developed anisotropy method, we set out to test if GSIS from grouped islets can be entrained during periodic application of CCh.

For this experiment, reagent reservoirs connected to inlets 1 and 2 contained 11 mM glucose and 10 μM CCh in 11 mM glucose, respectively. A group of five murine islets were loaded into the islet chamber that had been filled with 11 mM glucose. After sealing the chamber, islets were continuously perfused with constant 11 mM glucose from inlet 1. CCh pulses were generated by switching the flow from inlet 1 to inlet 2. Pulse profiles consisted of five pulses (denoted by "×" in Figure 4) each delivered for 30 s every 5 min. Considering broadening of each pulse (Figure 1C), islets were exposed to an effective CCh concentration of 4.7 μM.

As shown in Figure 4A, in the time prior to the first CCh pulse, only small insulin pulses were observed, which were likely due to the random overlap of insulin oscillations from the individual islets. Once the CCh pulses began, however, the measured insulin secretion profile was noticeably different. Whereas the first insulin spike after CCh delivery (labeled as peak 1 in Figure 4A) was slightly dampened, all four subsequent pulses induced significantly higher spikes of insulin. The total insulin secreted over the final three pulses (15−30 min experimental time) was 1600 pg. These CCh-potentiated oscillations promptly declined after delivery of the final pulse at 25 min.

To ensure that synchronization was due only to the periodic application of CCh and not to any feature of the microfluidic system itself, control experiments were performed by performing a similar pulse profile, but without CCh present. This ensured that the islets remained perfused with only 11 mM glucose even while the pulse profile was being delivered. As shown in Figure 4B, no discernible synchronization of insulin release was observed, only minor pulses similar to that observed prior to initiation of CCh pulses in the earlier experiment. A total of four control experiments were performed in this way, with the remaining three shown in Figure S6. These results complement our previous work[20] that showed potentiation and 1:1 entrainment of $[Ca^{2+}]_i$ by 5 min periodic CCh pulses.

CONCLUSIONS

Significant improvements to a previously described system were essential for allowing this online fluorescence anisotropy competitive insulin immunoassay to quantify biphasic GSIS dynamics from single and grouped pancreatic islets and for continued exploration of the hypothesis of ganglia-induced islet synchronization. The overall design of the microfluidic system produces subminute temporal resolution for insulin measurements, rapid enough to observe the fast oscillation dynamics of single islets. Key to improving the system was the use of SeTau-647 with its longer fluorescence lifetime than Cy5. This resulted in increased fluorescence emission depolarization and a greater anisotropy shift between low and high antigen concentrations. To demonstrate the applicability of the system, online dynamic insulin release from murine and human islets after glucose induction was measured. Synchronized GSIS from a group of islets entrained by periodic pulses of CCh was observed, providing new support for the hypothesis of ganglia-induced islet synchronization. Although our ensemble insulin secretion measurements do not currently allow for identifying potential heterogeneous effects among the pooled islets, future work could incorporate islet equivalent calculations to account for interislet heterogeneity. Implementation of an automated protocol to load islets into the device would also help to provide a more convenient platform for higher-throughput islet analyses. These shortcomings notwithstanding, our online homogeneous competitive immunoassay could be applicable as a user-friendly and affordable approach for the quantification of biologically relevant targets other than insulin with slight changes to the immunoassay reagents.

ASSOCIATED CONTENT

Supporting Information

The Supporting Information is available free of charge at https://pubs.acs.org/doi/10.1021/acs.analchem.0c01226.

Detailed figure of the perfusion system, detailed figure of the optical setup, derivation for calculated bound and free values, table of molecular weights and optical properties for the immunoassay reagents, examples single murine glucose stimulated insulin secretion profiles, examples of grouped murine glucose stimulated insulin secretion profiles, example of grouped human islet glucose stimulated insulin secretion profile, and control secretion profiles of grouped murine islets (PDF)

AUTHOR INFORMATION

Corresponding Author

Michael G. Roper − *Department of Chemistry and Biochemistry, Florida State University, Tallahassee, Florida 32306, United States*; orcid.org/0000-0002-0184-1333; Phone: 850-644-1846; Email: roper@chem.fsu.edu

Authors

Joel E. Adablah − *Department of Chemistry and Biochemistry, Florida State University, Tallahassee, Florida 32306, United States*

Yao Wang − *Department of Chemistry and Biochemistry, Florida State University, Tallahassee, Florida 32306, United States*

Matthew Donohue − *Department of Chemistry and Biochemistry, Florida State University, Tallahassee, Florida 32306, United States*

Complete contact information is available at: https://pubs.acs.org/10.1021/acs.analchem.0c01226

Notes

The authors declare the following competing financial interest(s): The authors have submitted an initial disclosure on this work.

https://dx.doi.org/10.1021/acs.analchem.0c01226
Anal. Chem. 2020, 92, 8464−8471

■ ACKNOWLEDGMENTS

We thank Wesley J. Eaton for his help with murine islet isolation and Julia Danyuk for her assistance in fabricating the microfluidic devices. This work was supported in part by grants from the National Institutes of Health, R01DK080714, and using resources and/or funding provided by the NIDDK-supported Human Islet Research Network (HIRN, RRID:SCR_014393; https://hirnetwork.org; UC4DK116283).

■ REFERENCES

(1) Chien, H. J.; Chiang, T. C.; Peng, S. J.; Chung, M. H.; Chou, Y. H.; Lee, C. Y.; Jeng, Y. M.; Tien, Y. W.; Tang, S. C. *Am. J. Physiol. Gastrointest. Liver Physiol.* **2019**, *317* (5), G694−G706.
(2) Bowles, A. C.; Ishahak, M. M.; Glover, S. J.; Correa, D.; Agarwal, A. *Integr. Biol.* **2019**, *11* (8), 331−341.
(3) Coronel, M. M.; Stabler, C. L. *Curr. Opin. Biotechnol.* **2013**, *24* (5), 900−908.
(4) Henquin, J. C. *Diabetologia* **2009**, *52* (5), 739−751.
(5) Shackman, J. G.; Dahlgren, G. M.; Peters, J. L.; Kennedy, R. T. *Lab Chip* **2005**, *5* (1), 56−63.
(6) Yi, L.; Bandak, B.; Wang, X.; Bertram, R.; Roper, M. G. *Anal. Chem.* **2016**, *88* (21), 10368−10373.
(7) Pørksen, N. *Diabetologia* **2002**, *45* (1), 3−20.
(8) Song, S. H.; McIntyre, S. S.; Shah, H.; Veldhuis, J. D.; Hayes, P. C.; Butler, P. C. *J. Clin. Endocrinol. Metab.* **2000**, *85* (12), 4491−4499.
(9) O'Rahilly, S.; Turner, R. C.; Matthews, D. R. *N. Engl. J. Med.* **1988**, *318* (19), 1225−1230.
(10) Matthews, D. R.; Naylor, B. A.; Jones, R. G.; Ward, G. M.; Turner, R. C. *Diabetes* **1983**, *32* (7), 617−621.
(11) Matveyenko, A. V.; Liuwantara, D.; Gurlo, T.; Kirakossian, D.; Dalla Man, C.; Cobelli, C.; White, M. F.; Copps, K. D.; Volpi, E.; Fujita, S.; et al. *Diabetes* **2012**, *61* (9), 2269−2279.
(12) Molina, J.; Rodriguez-Diaz, R.; Fachado, A.; Jacques-Silva, M. C.; Berggren, P. O.; Caicedo, A. *Diabetes* **2014**, *63* (8), 2714−2726.
(13) Satin, L. S.; Kinard, T. A. *Endocrine J.* **1998**, *8* (3), 213−223.
(14) King, B. F.; Love, J. A.; Szurszewski, J. H. *J. Physiol.* **1989**, *419* (1), 379−403.
(15) Stagner, J. I.; Samols, E. *Am. J. Physiol.* **1985**, *248* (5), E522−E530.
(16) Stagner, J. I.; Samols, E.; Weir, G. C. *J. Clin. Invest.* **1980**, *65* (4), 939−942.
(17) Goodner, C. J.; Koerker, D. J.; Stagner, J. I.; Samols, E. *Am. J. Physiol.* **1991**, *260* (3), E422−E429.
(18) Gylfe, E.; Grapengiesser, E.; Dansk, H.; Hellman, B. *Pancreas* **2012**, *41* (2), 258−263.
(19) Zhang, M.; Fendler, B.; Peercy, B.; Goel, P.; Bertram, R.; Sherman, A.; Satin, L. S. *Biophys. J.* **2008**, *95* (10), 4676−4688.
(20) Adablah, J. E.; Vinson, R.; Roper, M. G.; Bertram, R. *PLoS One* **2019**, *14* (2), e0211832.
(21) Roper, M. G.; Shackman, J. G.; Dahlgren, G. M.; Kennedy, R. T. *Anal. Chem.* **2003**, *75* (18), 4711−4717.
(22) Dishinger, J. F.; Reid, K. R.; Kennedy, R. T. *Anal. Chem.* **2009**, *81* (8), 3119−3127.
(23) Yi, L.; Wang, X.; Dhumpa, R.; Schrell, A. M.; Mukhitov, N.; Roper, M. G. *Lab Chip* **2015**, *15* (3), 823−832.
(24) Shigeto, H.; Ikeda, T.; Kuroda, A.; Funabashi, H. *Anal. Chem.* **2015**, *87* (5), 2764−2770.
(25) Hu, J.; Easley, C. J. *Anal. Chem.* **2017**, *89* (16), 8517−8523.
(26) Hu, J.; Wang, T.; Kim, J.; Shannon, C.; Easley, C. J. *J. Am. Chem. Soc.* **2012**, *134* (16), 7066−7072.
(27) Nithipatikom, K.; McGown, L. B. *Talanta* **1989**, *36* (1−2), 305−309.
(28) Schrell, A. M.; Mukhitov, N.; Yi, L.; Adablah, J. E.; Menezes, J.; Roper, M. G. *Anal. Methods* **2017**, *9* (1), 38−45.
(29) Glieberman, A. L.; Pope, B. D.; Zimmerman, J. F.; Liu, Q.; Ferrier, J. P.; Kenty, J. H. R.; Schrell, A. M.; Mukhitov, N.; Shores, K. L.; Tepole, A. B.; et al. *Lab Chip* **2019**, *19* (18), 2993−3010.
(30) Li, X.; Hu, J.; Easley, C. J. *Lab Chip* **2018**, *18* (19), 2926−2935.
(31) Hu, J.; Li, X.; Judd, R. L.; Easley, C. J. *Lab Chip* **2020**, *20* (8), 1503−1512.
(32) Jameson, D. M.; Ross, J. A. *Chem. Rev.* **2010**, *110* (5), 2685−2708.
(33) Zhang, H.; Wu, Q.; Berezin, M. Y. *Expert Opin. Drug Discovery* **2015**, *10* (11), 1145−1161.
(34) Lakowicz, J. R. *Principles of Fluorescence Spectroscopy*, 3rd ed.; Springer: New York, 2006; pp 353−382.
(35) Mukhitov, N.; Adablah, J. E.; Roper, M. G. *Islets* **2019**, *11* (2), 21−32.
(36) Wang, X.; Roper, M. G. *Anal. Methods* **2014**, *6* (9), 3019−3024.
(37) Lomasney, A. R.; Yi, L.; Roper, M. G. *Anal. Chem.* **2013**, *85* (16), 7919−7925.
(38) Bandak, B.; Yi, L.; Roper, M. G. *Lab Chip* **2018**, *18* (18), 2873−2882.
(39) Schrell, A. M.; Mukhitov, N.; Roper, M. G. *Anal. Chem.* **2016**, *88* (16), 7910−7915.
(40) *Fluorescent Tools for BioMedical Applications Product name: SeTau-647-NHS General Data. SETA BioMedicals*. http://www.setabiomedicals.com (accessed 2020-01-14).
(41) Oswald, B.; Patsenker, L.; Duschl, J.; Szmacinski, H.; Wolfbeis, O. S.; Terpetschnig, E. *Bioconjugate Chem.* **1999**, *10* (6), 925−931.
(42) Xiao, S.; Fu, N.; Peckham, K.; Smith, B. D. *Org. Lett.* **2010**, *12* (1), 140−143.
(43) Huang, Z.; Ji, D.; Wang, S.; Xia, A.; Koberling, F.; Patting, M.; Erdmann, R. *J. Phys. Chem. A* **2006**, *110* (1), 45−50.
(44) Widengren, J.; Schwille, P. *J. Phys. Chem. A* **2000**, *104* (27), 6416−6428.
(45) Luschtinetz, F.; Dosche, C.; Kumke, M. U. *Bioconjugate Chem.* **2009**, *20* (3), 576−582.
(46) Webster, S.; Fu, J.; Padilha, L. A.; Przhonska, O. V.; Hagan, D. J.; Van Stryland, E. W.; Bondar, M. V.; Slominsky, Y. L.; Kachkovski, A. D. *Chem. Phys.* **2008**, *348* (1−3), 143−151.
(47) Henquin, J. C.; Dufrane, D.; Nenquin, M. *Diabetes* **2006**, *55* (12), 3470−3477.
(48) Cabrera, O.; Jacques-Silva, M. C.; Berman, D. M.; Fachado, A.; Echeverri, F.; Poo, R.; Khan, A.; Kenyon, N. S.; Ricordi, C.; Berggren, P. O.; et al. *Cell Transplant.* **2007**, *16* (10), 1039−1048.
(49) Henquin, J.-C.; Dufrane, D.; Kerr-Conte, J.; Nenquin, M. *Am. J. Physiol. Metab.* **2015**, *309* (7), E640−E650.
(50) Lenguito, G.; Chaimov, D.; Weitz, J. R.; Rodriguez-Diaz, R.; Rawal, S. A. K.; Tamayo-Garcia, A.; Caicedo, A.; Stabler, C. L.; Buchwald, P.; Agarwal, A. *Lab Chip* **2017**, *17* (5), 772−781.

■ NOTE ADDED AFTER ASAP PUBLICATION

Panels A and B of Figure 4 were switched in the original version published on June 3, 2020. The corrected version was reposted on June 5, 2020.

https://dx.doi.org/10.1021/acs.analchem.0c01226
Anal. Chem. 2020, 92, 8464−8471